Observation of two-α emission from high-lying excited states of ^{18}Ne by complete-kinematics measurements

X. X. Xu,* C. J. Lin, H. M. Jia, F. Yang, F. Jia, Z. D. Wu, S. T. Zhang, Z. H. Liu, and H. Q. Zhang
China Institute of Atomic Energy, Beijing 102413, People's Republic of China

H. S. Xu, Z. Y. Sun, J. S. Wang, Z. G. Hu, M. Wang, R. F. Chen, X. Y. Zhang, C. Li, X. G. Lei, Z. G. Xu, G. Q. Xiao, and W. L. Zhan
Institute of Modern Physics, The Chinese Academy of Science, Lanzhou 73000, People's Republic of China
(Received 11 July 2010; revised manuscript received 7 September 2010; published 27 December 2010)

Two-α emission from high-lying excited states of ^{18}Ne was studied by complete-kinematics measurements. The ^{18}Ne beam at the energy of 51.8 MeV/u was bombarding a ^{197}Au target to populate the excited states via Coulomb excitation. Products of two-α emission, ^{10}C-α-α, were measured by an array of silicon strip detectors and a CsI + PIN telescope. With the help of Monte Carlo simulations, the experimental results show the characteristics of sequential two-α emission via ^{14}O excited states. Sequential two-α and two-proton emissions from ^{18}Ne via one-particle daughter states are compared and the distinction of the opening angles of these two modes originates from the difference of the mass ratio of emitted particles to daughter nuclei.

DOI: 10.1103/PhysRevC.82.064316 PACS number(s): 23.60.+e, 25.60.−t, 25.70.−z, 27.20.+n

I. INTRODUCTION

Two-particle correlation measurements were used to study the properties of highly excited nuclear systems over the last few decades. Following the discovery of rotational band structure in ^{20}Ne, two-α (2α) angular correlations were measured first to assign the spins for high-lying excited levels in the ^{12}C(^{12}C,α)^{20}Ne reaction [1]. Later, different α-α angular correlation methods were widely applied to deduce quantum numbers for resonances in the continuum of ^{20}Ne [2,3] and ^{24}Mg [4,5]. Moreover, two-particle relative-momentum correlation functions can provide information about the space-time characteristic of the emitting system [6,7]. In the ^{40}Ar- [8] and ^{16}O- [9] induced reactions on the ^{197}Au target, although the α-α correlation functions were dominated by the decay of the ^{8}Be ground state [$J^{\pi} = 0^{+}$, $\Gamma = 6.8$ eV], the distributions still showed a broad peak at about 105 MeV/c corresponding to the first excited state [$E^{*} = 3.04$ MeV, $J^{\pi} = 2^{+}$, $\Gamma = 1.5$ MeV] of ^{8}Be. ^{8}Be emission, with a substantially higher Coulomb barrier than ^{4}He, may be related to the exotic structure of the decay states in these nuclei.

With the development of new detection techniques [10], complete-kinematics measurements can be achieved and two-particle correlations in the exotic emission have been proven to be a versatile tool to study the breakup of a quantum system into three particles, for instance, in the cases of ^{9}Be ($5/2^{-}$) [11] and ^{12}C (1^{+}) [12]. Generally speaking, the distinction of the three-body breakup can usually be made between direct and sequential two-body decay. In the direct breakup, three particles simultaneously leave the interaction region, and dynamical correlations between them can be observed experimentally. In contrast, sequential two-body decay is realized via a one-particle daughter state or a resonance of two particles. The only correlation originates from conservation laws for the sequential emission.

The radioactive nuclei close to and beyond the proton drip line provide a flexible platform for the study of the three-body breakup which was primarily focused on core-proton-proton configurations, such as two-proton ($2p$, fermions) emission from ^{18}Ne [13,14], ^{29}S [15], and ^{28}P [16]. Here we present studies of the three-body breakup of ^{18}Ne with another configuration, i.e., two-α (bosons) emission from excited states by complete-kinematics measurements.

II. EXPERIMENTAL DETAILS

The experiment was performed at the National Laboratory of Heavy Ion Research (HIRFL) of the Institute of Modern Physics, Lanzhou, China. A primary beam ^{20}Ne at an energy of 78.2 MeV/u and an average intensity of 10 pnA, was extracted from the Separate Sector Cyclotron (SSC) and fragmented on a ^{9}Be target with a thickness of 1590 μm. A radioactive ion beam (RIB) of $E/A = 51.8$ MeV ^{18}Ne was separated and purified by the RIB line [Radioactive Ion Beam Line in Lanzhou (RIBLL)] spectrometer [17] using the combined $B\rho$-ΔE-$B\rho$ method. The schematic diagram of the detector setup is plotted in Fig. 1. Secondary ions, with an intensity of 10^{4} ions/s RIBs mixture and a purity of ^{18}Ne at 35%, were identified by using the time of flight (TOF) and energy loss (ΔE). TOF was measured by two plastic scintillators placed on the second and fourth focus planes of the RIBLL spectrometer and ΔE was obtained with a silicon detector (SD0). Figure 2 shows a two-dimensional fragment identification spectrum of ΔE versus TOF. A total of 2.1×10^{8} ^{18}Ne events were accumulated in the experiment. Then RIBs impinged on a secondary target, ^{197}Au, with a thickness of 383.9 mg/cm^{2}. Two parallel-plate avalanche counters fixed in front of the ΔE detector were used to reconstruct the interaction point of each fragment incident on the target. A

*xuxinxing@ciae.ac.cn

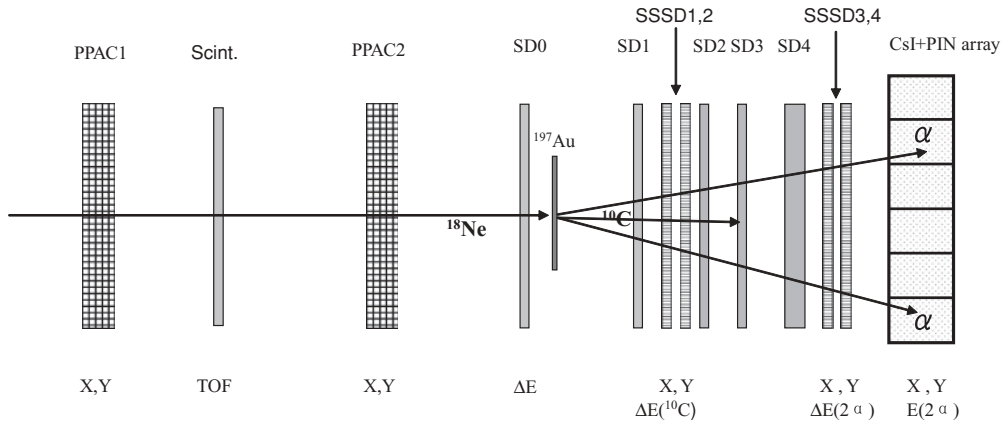

FIG. 1. The schematic diagram of the detector setup designed for the study of exotic emissions of ^{18}Ne by the complete-kinematics measurement.

detector array was mounted behind the secondary target in order to achieve complete-kinematics measurements of all the reaction products. This setup consisted of a sequence of eight silicon detectors and 6 × 6 CsI crystals. As shown in Fig. 1, SD is a large-area silicon detector (SD0,1,2,3: 325 μm and SD4: 1000 μm) and SSSD is a single-sided silicon strip detector (300 μm thick, 24 strips, 2 mm wide with a 0.1-mm interval). SSSD1,2 were placed in a crossed geometry to provide x -y measurements for heavy fragments and SSS3,4 for light particles. Each CsI crystal (15 × 15 × 20 mm) was coupled with PIN photodiodes for reading out. An opening angle covered by the detector array in the laboratory was ±11° in this arrangement.

Measurements of energies and scattering angles of light particles produced in reactions were achieved by a multiple-stack telescope in the detector array. Light particles passed through silicon detectors and stopped in the CsI crystals. SSSD3,4 and SD4 were used for energy-loss measurements of the emitted light particles. The residual energy was measured by the CsI + PIN detectors. Calibration of these detectors was achieved by light-particle beams at different energies originating from the projectile fragmentation with the $B\rho$ setting for light-particle transmission. Figure 3 displays an identification spectrum of light particles emitted from the excited states of ^{18}Ne. For single-particle emission in Fig. 3(a), one can clearly see proton and deuteron bands, and barely a triton band. A ^{4}He band can also be seen at higher values of the energy loss and residual energy. The ^{3}He band could hardly be detected. In Fig. 3(b), the double hits correspond to two particles in two different CsI crystals in the same event. The plotted quantities are the sum of the energy losses of the two particles in SSSD4, and the sum of the two CsI energies. 2α emission events were unambiguously identified from other two-particle emission events by the ΔE-E_r method. Although some bands, such as proton-proton and proton-deuteron events, cannot be separated in Fig. 3(b), the two particles of each band can be identified, respectively, by the ΔE versus E_r matrix of the single particle in Fig. 3(a).

The heavy fragments, such as ^{18}Ne, ^{14}O, and ^{10}C, were identified and tracked by another multiple telescope composed of SD1, SSSD1,2, and SD2,3 for measurements of the energy loss and residual energy. These silicon detectors were calibrated using the secondary ions produced by the primary beam ^{20}Ne, such as ^{20}Na, ^{17,18}F, and ^{16}O with the $B\rho$ setting for transmission. In order to get higher-energy ions during the calibration of each silicon detector, the ^{27}Al degrader after the

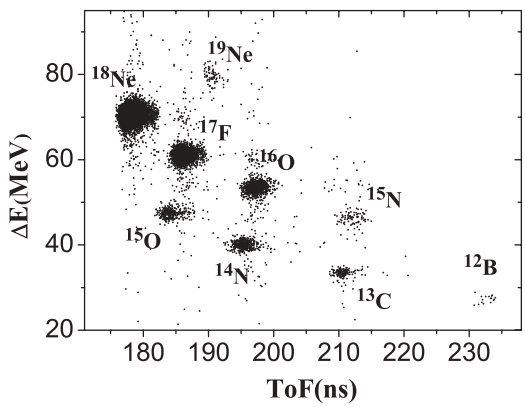

FIG. 2. Particle identification spectrum of energy loss from a large-area silicon detector versus time of flight between the two plastic scintillators for RIBs.

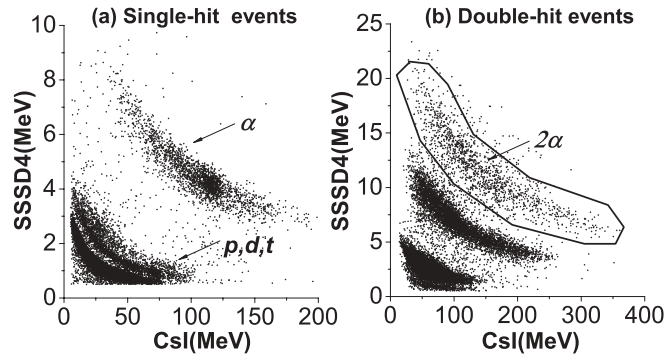

FIG. 3. Light particle identification spectra from the detector array. The energy loss in the SSSD4 is plotted as a function of the residual energy in the CsI + PIN detector array. (a) One-fifth of one-particle emission events and (b) total two-particle emission events from the excited states of ^{18}Ne.

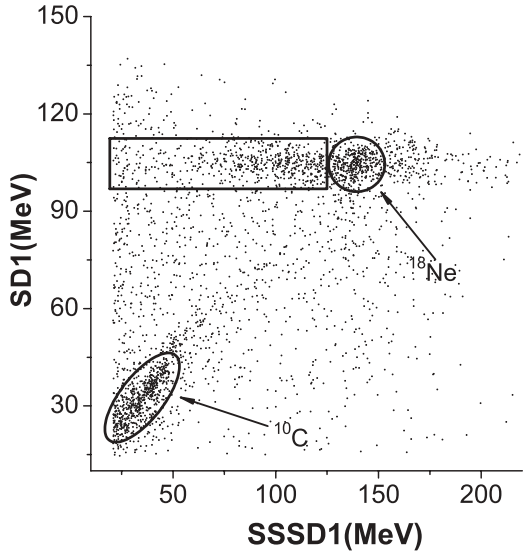

FIG. 4. Two-dimensional matrix for the identification of the heavy fragments from the excited states of ^{18}Ne by the energy losses of SD1 versus SSSD1, which is coincident with the 2α gate in Fig. 3(b). The daughter nuclei ^{10}C of the reactions on the secondary target are unambiguously identified.

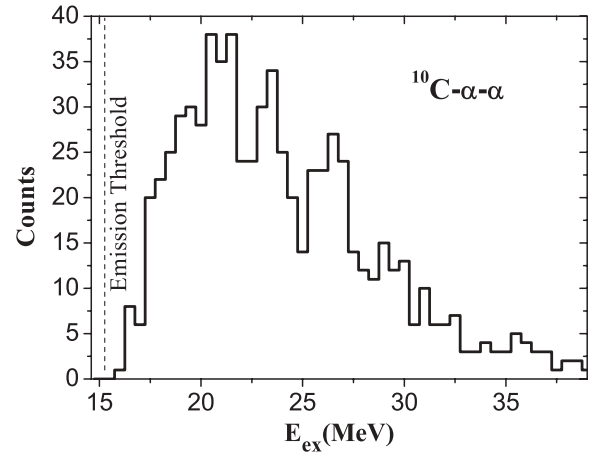

FIG. 5. Reconstructed excitation-energy spectrum for ^{18}Ne from three-body correlations of ^{10}C-α-α events.

^{9}Be target was removed. Figure 4 displays the identification of the daughter nucleus of 2α emission from the excited states of ^{18}Ne by the energy losses of SD1 versus SSSD1. Compared with the energy-loss calculation by the program LISE [18], ions of ^{18}Ne and ^{10}C were identified and displayed in the circle and ellipse regions, respectively. The two-dimensional identification plot provided the reaction information in detail. The events in the ellipse represented the reactions on the secondary target. When the reactions took place on SSSD2 and SD2, the ions could be identified as ^{18}Ne by the energy losses of SD1 versus SSSD1, as shown in the circle. The events in the rectangle originated from the breakup on SSSD1 and those from reactions on SD1 were distributed over the area between the rectangle and the ellipse.

III. DATA ANALYSIS AND RESULTS

A. Identification of the reaction channel of 2α emission

The ^{10}C-α-α coincidences were carried out event by event for the analysis of 2α emission from the excited states of ^{18}Ne. First, the parent nucleus ^{18}Ne was selected on the two-dimensional RIB identification spectrum of ΔE (SD0) versus TOF (see Fig. 2). Second, the events within the 2α gate were identified by the ΔE (SSSD4) versus E_r (CsI) matrix (see Fig. 3). Finally, identification of the decay daughter nucleus, ^{10}C, was achieved with the two-dimensional ΔE spectrum of SD1 as a function of SSSD1 (see Fig. 4). After the selection procedure, about 700 events of 2α correlations emitted from the excited states of ^{18}Ne were identified totally.

B. Experimental results and Monte Carlo simulations

In the present experiment, the opening angle ($\theta_{\alpha\alpha}^{\mathrm{c.m.}}$), the relative momentum ($q_{\alpha\alpha} = |\mathbf{p}_1 - \mathbf{p}_2|/2$), the excited states ($E_{\mathrm{ex}}$), or the invariant mass of decay products in the center-of-mass system of the parent nucleus ^{18}Ne have been reconstructed by kinematical analyses. Resolutions of these observing variables were determined by energy and position resolutions of the detector array. The energy signals from silicon detectors included the energy losses of both heavy fragments, ^{10}C, and light particles. We calculated the energy losses of two α's in each silicon detector using the residual energies in the CsI crystals and the program LISE [18]. Thus, as displayed in Fig. 4 the energy loss of the daughter nucleus was deduced. In addition, a small fraction of the total kinematical energy (TKE) of ^{10}C deposited in SD4. This fraction of the TKE could be calculated via energy losses in silicon detectors before SD4 in a similar way. With these arrangements and the resolutions of the detectors taken into consideration, the resolutions of the experimental setup are about 500 KeV for E_{ex}, 5° for $\theta_{\alpha\alpha}^{\mathrm{c.m.}}$, and 5 MeV/$c$ for $q_{\alpha\alpha}$, respectively.

Figure 5 displays the excitation-energy spectra of ^{18}Ne reconstructed from ^{10}C-α-α events. Several resonance states are visible at excitation energies of 20.7, 23.3, and 26.2 MeV. These states are so high that their excitation energies and configurations have not been precisely measured in experiments. In order to investigate 2α correlations from the high-lying excited states, one of the excitation-energy regions, $24.6 < E_{\mathrm{ex}} < 28.1$ MeV, was chosen to study in detail. The $\theta_{\alpha\alpha}^{\mathrm{c.m.}}$ and $q_{\alpha\alpha}$ distributions for this excitation-energy region are shown in Fig. 6. The experimental data show an enhancement at angles greater than 90° for $\theta_{\alpha\alpha}^{\mathrm{c.m.}}$. The angular correlations are different from others, such as the opening angle of 2p emission (isotropic or enhanced at angles less than 90°) [14–16]. The $q_{\alpha\alpha}$ covers the area from 30 to 210 MeV/c and reaches a maximum at 150 MeV/c.

In order to reproduce the experimental data, Monte Carlo (MC) simulations of sequential two-body emission were carried out. Because the energies, spins, and parities of the high-lying initial levels, as well as some intermediate and final states, were still unknown, the accurate calculation including the configurations of these states could not be realized. Instead, simple sequential emission via one-α daughter states (^{14}O*)

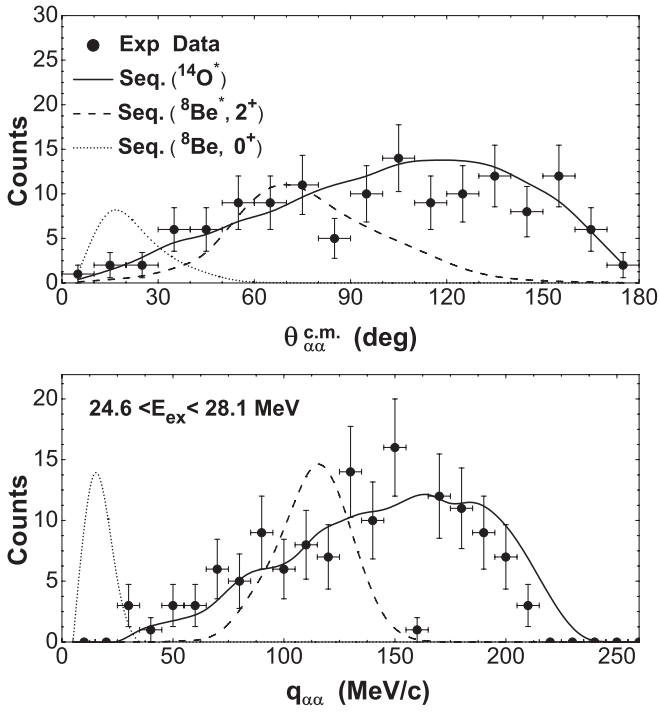

FIG. 6. Distributions of the opening angle (top) and the relative momentum (bottom) of two-α emission from an excitation-energy region of ^{18}Ne, 24.6 $< E_{ex} <$ 28.1 MeV, show sequential two-body emission via ^{14}O excited states.

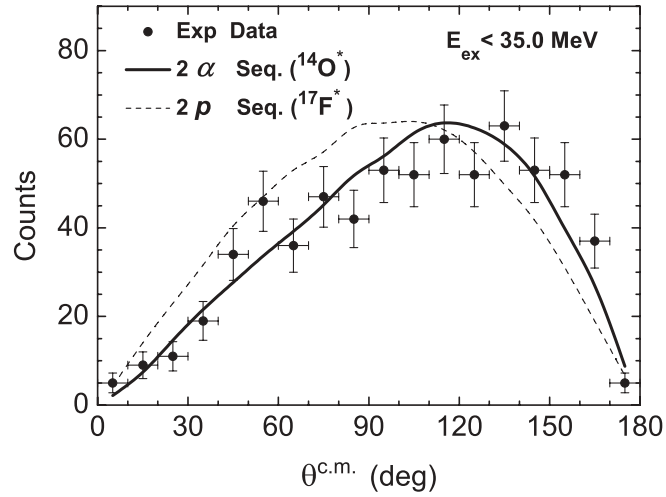

FIG. 7. The opening angle of two-α emission from excited states of the nucleus ^{18}Ne less than 35.0 MeV and the simulative comparison of two-α with two-proton emissions via one-particle daughter states display the influence of the mass ratio of emitted particles to daughter nuclei on the distribution of $\theta^{c.m.}$.

or a resonance of two α's (^{8}Be: 0^{+}, 2^{+}) was simulated in the code. The possible α-decaying candidate states in ^{14}O were 10.89, 11.24, 11.97, 12.84, 13.01 MeV, and so on [19]. The distributions of $\theta^{c.m.}_{\alpha\alpha}$ and $q_{\alpha\alpha}$ were not so sensitive to the branching ratios of intermediate states in ^{14}O. The energies of initial levels were obtained by using the method of Gaussian curve approximation to fit the distribution of the excitation-energy region, 24.6 $< E_{ex} <$ 28.1 MeV. Isotropic emission [a flat distribution for cos(θ) between $-$ 1 and 1, φ between 0° and 360°, respectively, in spherical coordinates] from the excitation-energy region of ^{18}Ne was taken into consideration in the MC code, which was similar to the simulation of 2p emission from ^{17}Ne [20,21]. This means that the possible angular correlations due to the angular momentum and parity conservation were neglected. In the simulation, the energy and position resolutions of detectors, the experimental setup, and Coulomb deflections of heavy fragments were also taken into account. The MC simulation showed basically the character of sequential two-α emission via ^{14}O excited states from the ^{18}Ne excitation-energy region, 24.6 $< E_{ex} <$ 28.1 MeV (see Fig. 6); the solid, short-dotted, and dashed curves represent the sequential emissions via ^{14}O excited states, ^{8}Be (0^{+}), and ^{8} Be (2^{+}), respectively. Figure 7 displays the similar distribution of $\theta^{c.m.}_{\alpha\alpha}$ of two α's emitted from excited states less than 35.0 MeV of the nucleus ^{18}Ne and the data were also described by the sequential 2α emission via ^{14}O excited states.

MC simulations showed that the detection efficiencies were about 49.0, 30.6, and 52.1% for the sequential emissions via ^{14}O excited states, ^{8}Be (0^{+}), and ^{8}Be (2^{+}), respectively. As the pairs of α particles from the ground state of ^{8}Be [Q (α) = 91.8 KeV] came out very closely in the laboratory, 65.2% of them would be detected by the detector array, and 34.6% hit a single CsI crystal. Therefore, identification of 2α coincidences that required two separate CsI crystals resulted in a much lower efficiency for ^{8}Be (0^{+}) emission than the others. 2α positions were obtained by both CsI detectors and SSSD3,4. Although the smallest opening angle of CsI detectors (3.6°) was unsuitable for the measurements of ^{8}Be nuclei in their ground state, position resolutions of SSSD3,4 (0.9°) were good enough to actually identify them. The experimental results reconstructed by the SSSD3,4 also showed the nonobservation of emitted ^{8}Be nuclei and kept consistent with the distribution of the observing variables deduced by the CsI detector array.

Although the sequential approach was simple and further studies of correlations resulting from the conservation of angular momentum and parity would be required, the simulation of sequential 2α emission via ^{14}O excited states reproduced the enhancement at angles greater than 90° for $\theta^{c.m.}_{\alpha\alpha}$. In addition, a simulation of sequential 2p emission via 1p daughter states from the same energy levels of ^{18}Ne showed a nearly isotropic distribution for $\theta^{c.m.}_{pp}$. It indicated that variations of the mass ratio of emitted particles to daughter nuclei (m_p/m_d) are chiefly responsible for the different distributions of $\theta^{c.m.}$. For instance, in an extreme case, $m_p/m_d \gg 1$ (emitted particles are in fact much heavier than the daughter), the opening angle would have the distribution of a maximum at 180°. And in the former experiment of ^{12}O [22,23], the distribution of $\theta^{c.m.}_{pp}$ of sequential 2p emission showed a slight enhancement at angles greater than 90° with a small value of m_p/m_d close to zero. Therefore, with the increases of the m_p/m_d values, the peaks of the opening angle distribution for two particles sequentially emitted from the parent nucleus would move to large angles in the interval [90°,180°] due to kinematical effects, which has been reproduced well by the MC simulations.

IV. CONCLUSION

In summary, we performed the first complete-kinematics experiment of two-α emission from high-lying excited states of ^{18}Ne. The experimental results combined with simple MC simulations show sequential 2α emission via ^{14}O excited states. The distribution of $\theta_{\alpha\alpha}^{\mathrm{c.m.}}$ shows an enhancement at angles greater than 90°. Compared with the opening angle of $2p$ emission, it is the ratio of m_p/m_d that results in the different distribution for $\theta^{\mathrm{c.m.}}$ in sequential two-body emission.

To understand the delicate relevance between nuclear structure and two-α emission, the highly precise energy levels and their configurations of ^{18}Ne are required to be measured in experiments. In addition, the direct breakup calculated by strict three-body theories are needed for 2α emission although the sequential model fits the data.

ACKNOWLEDGMENTS

We acknowledge the continuous effort of the HIRFL-RIBLL operators for providing good-quality beams, ensuring compatibility of the electronics and the data acquisition system. This work was supported by the National Natural Science Foundation of China under Grants No. 10675169, No. 10735100, No. 10727505, and No. 11005156 and the Major State Basic Research Developing Program under Grant No. 2007CB815003.

[1] J. A. Kuehner, Phys. Rev. **125**, 1650 (1962).
[2] L. K. Fifield, R. W. Zurmühle, D. P. Balamuth, and J. W. Noé, Phys. Rev. C **8**, 2203 (1973).
[3] W. D. M. Rae, P. R. Keeling, and S. C. Allcock, Phys. Lett. B **184**, 133 (1987).
[4] L. K. Fifield, R. W. Zurmühle, and D. P. Balamuth, Phys. Rev. C **8**, 2217 (1973).
[5] K. C. Young Jr., J. M. Lind, R. W. Zurmühle, and D. P. Balamuth, Nucl. Phys. A **323**, 178 (1979).
[6] M. A. Bernstein *et al.*, Phys. Rev. Lett. **54**, 402 (1985) and references therein.
[7] J. Pochodzalla, C. B. Chitwood, D. J. Fields, C. K. Gelbke, W. G. Lynch, M. B. Tsang, D. H. Boal, and J. C. Shillcock, Phys. Lett. B **174**, 36 (1986) and references therein.
[8] J. Pochodzalla *et al.*, Phys. Rev. C **35**, 1695 (1987).
[9] Z. Chen *et al.*, Phys. Rev. C **36**, 2297 (1987).
[10] B. Blank and M. J. G. Borge, Prog. Part. Nucl. Phys. **60**, 403 (2008) and references therein.
[11] R. Álvarez-Rodríguez, H. O. U. Fynbo, A. S. Jensen, and E. Garrido, Phys. Rev. Lett. **100**, 192501 (2008) and references therein.
[12] H. O. U. Fynbo *et al.*, Phys. Rev. Lett. **91**, 082502 (2003).
[13] J. Gómez del Campo *et al.*, Phys. Rev. Lett. **86**, 43 (2001).
[14] G. Raciti, G. Cardella, M. De Napoli, E. Rapisarda, F. Amorini, and C. Sfienti, Phys. Rev. Lett. **100**, 192503 (2008).
[15] C. J. Lin *et al.*, Phys. Rev. C **80**, 014310 (2009).
[16] X. X. Xu *et al.*, Phys. Rev. C **81**, 054317 (2010).
[17] Z. Sun, W.-L. Zhan, Z.-Y. Guo, G. Xiao, and J.-X. Li, Nucl. Instrum. Methods Phys. Res. A **503**, 496 (2003).
[18] D. Bazin, O. Tarasov, M. Lewitowicz, and O. Sorlin, Nucl. Instrum. Methods Phys. Res. A **482**, 307 (2002).
[19] G. C. Ball and J. Cerny, Phys. Rev. **155**, 1170 (1967).
[20] T. Zerguerras, Ph.D. thesis, Institute de Physique Nucléaire Orsay, 2001.
[21] T. Zerguerras *et al.*, Eur. Phys. J. A **20**, 389 (2004).
[22] R. A. Kryger *et al.*, Phys. Rev. Lett. **74**, 860 (1995).
[23] A. Azhari, R. A. Kryger, and M. Thoennessen, Phys. Rev. C **58**, 2568 (1998).